

# Long-range attraction of particles adhered to lipid vesicles

Raphael Sarfati<sup>1,2</sup> and Eric R. Dufresne<sup>3,1,4</sup>

<sup>1</sup>*Department of Applied Physics, Yale University, New Haven, CT 06511*

<sup>2</sup>*Integrated Graduate Program in Physical and Engineering Biology, Yale University*

<sup>3</sup>*Department of Materials, ETH Zürich, 8092 Zürich, Switzerland*

<sup>4</sup>*School of Engineering and Applied Science, Yale University*

Many biological systems fold thin sheets of lipid membrane into complex three-dimensional structures. This microscopic origami is often mediated by the adsorption and self-assembly of proteins on a membrane. As a model system to study adsorption-mediated interactions, we study the collective behavior of micrometric particles adhered to a lipid vesicle. We estimate the colloidal interactions using a maximum likelihood analysis of particle trajectories. When the particles are highly wrapped by a tense membrane, we observe strong long-range attractions with a typical binding energy of  $150 k_B T$  and significant forces extending a few microns.

The geometry of lipid membranes is essential to living cells. Their topology defines the boundaries of the cell, nucleus, and organelles [1]. Their shape and size also play an essential role in cellular physiology, from the contraction of muscle [2] to the creation of vivid structural color [3]. Therefore, regulation of membrane geometry is of fundamental importance to cell biology.

In many cases, the folding of lipid membranes into complex three-dimensional structures is achieved by the adsorption and self-assembly of proteins on the surface of a lipid membrane [4]. While many of the essential molecules have been identified, relatively little is known about the basic physics of protein-assisted membrane folding. Experiments have demonstrated a coupling between membrane curvature and binding affinity [5]. Furthermore, membrane folding is intimately related to the organization of adsorbed proteins into supermolecular structures [4]. These observations have inspired a number of theoretical studies considering the adsorption and interaction of proteins on membranes [6, 7]. However, experimental measurements of the interactions of membrane-bound proteins are unavailable.

The mechanics of bare lipid membranes is a compromise of tension and bending energy [8, 9]. When particles adsorb, the physics is enriched by the particles' adhesion energy and geometry. More precisely, for a piece of membrane of shape  $\mathcal{S}$  with a bound particle, the energy of the system is described by the Helfrich Hamiltonian

$$\mathcal{H}(\mathcal{S}) = -w a_c + \int \left( \sigma + \frac{1}{2} \kappa C^2 \right) dA, \quad (1)$$

where  $\sigma$  is the membrane tension,  $\kappa$  the bending rigidity,  $C$  the local total curvature, and  $w$  and  $a_c$  the adhesive surface energy and area of contact between the membrane and the particle. An important material length scale emerges,  $\lambda = \sqrt{\kappa/\sigma}$ . Bending dominates on shorter scales, and tension dominates on longer ones. Bending rigidities of lipid bilayers are typically around  $20 k_B T$ , so for moderately tensed vesicles ( $\sigma \sim 10^{-5} - 10^{-4}$  N/m),  $\lambda \sim 50\text{-}100$  nm [10].

While membrane-mediated interactions of bound proteins are challenging to access experimentally, a few studies have made qualitative observations of membrane-induced attractions between micrometric colloidal particles [11, 12]. These observations are not consistent with analytical theories of particle interactions that assume small deformations and predict repulsive interactions [13]. On the other hand, numerical studies in the large deformation regime find attractions [6, 14, 15], in concert with the existing experimental data.

In this article, we investigate the interactions of membrane-bound particles using micron-sized colloidal particles attached to a giant unilamellar vesicle (GUV). When particles are highly wrapped by a tense membrane, they spontaneously aggregate. We introduced a maximum likelihood analysis to estimate the pair potential from the approach to binding of individual particle pairs. The potential is strongly attractive ( $> 100 k_B T$  deep), and long-ranged ( $> 4 \mu\text{m}$ ).

## EXPERIMENTAL RESULTS

Giant unilamellar vesicles of POPC (98%), enhanced with lipids functionalized by rhodamine (1%) and PEG-biotin (1%), are fabricated by electroformation [16]. They are re-suspended in a hypotonic buffer, and settle onto a non-adherent coverslip. The vesicles have a wide range of tensions: some exhibit large shape fluctuations, while others are smooth and nearly spherical (Fig. 1A). Using optical tweezers (1064 nm), we bring streptavidin-functionalized polystyrene spheres (radius  $R = 1 \mu\text{m}$ ) in contact with GUVs of diameter from  $15 \mu\text{m}$  to  $20 \mu\text{m}$ . There is strong adhesion of the particles to the bilayer due to the interaction of biotin with streptavidin. The extent of adhesion varies somewhat from bead to bead, but membrane typically wraps the bead past its equator, as shown in Fig. 1A.

Even though individual particles are stable in the bulk, beads bound to tense GUVs formed clusters, as shown by the micrograph in Fig. 1C. Thermal fluctuations were

not able to dismantle these clusters, but they did cause significant fluctuations in the particle separation, as we will discuss later.

These particle interactions are long-ranged. Particles within a few microns of one another move quasi-ballistically toward a bound state, as shown in the time sequence in Fig. 1(D-E-F). We imaged the approach of particle pairs with a high-speed camera (250 frames per second) and extracted the bead positions using a standard particle tracking algorithm [17]. Three representative trajectories of the center-to-center separation between two  $2\text{-}\mu\text{m}$ -diameter beads bound to the same vesicle are shown in Fig. 2. All show a strong attraction starting from over  $4\text{ }\mu\text{m}$  away, with average velocities around  $1\text{ }\mu\text{m/s}$ , and significant fluctuations about a bound state near contact. A movie showing the approach and binding of a pair of particles is available in the Supporting Information.

### MAXIMUM LIKELIHOOD ANALYSIS

We aim to quantify these membrane-mediated interactions. Analysis of the fluctuations near equilibrium [18] enable measurement of the stiffness of the particle-particle bond, but do not sample the long-range interaction. In principle, the long-range interaction could be probed using optical tweezers as a force transducer [19], or blinking optical tweezers [17, 20]. Unfortunately, we have found that lipid vesicles are perturbed by the laser traps; however, they relax after about 200 ms after the laser is blocked.

Consequently, we introduce an alternate approach to

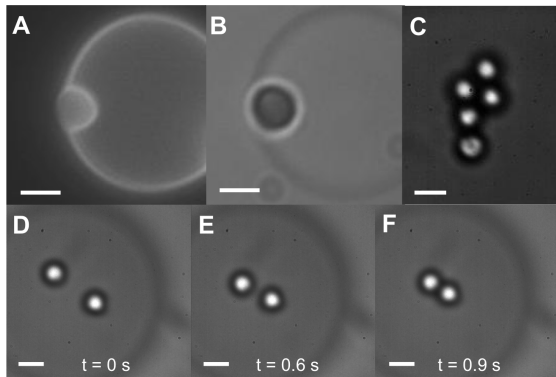


FIG. 1. Particle binding and interaction on GUVs. Scale bar is  $2\text{ }\mu\text{m}$ . (A) Fluorescent and (B) corresponding brightfield images of a bead strongly bound to the equatorial plane of a vesicle. More than half of the particle's surface appears to be wrapped. The GUV is tense, since its shape is spherical and no undulations are visible. (C) Particles self-assemble when bound to the same GUV. (D-E-F) Time sequence of two particles at the top of a GUV ( $18\text{ }\mu\text{m}$  diameter) interacting across a distance of over  $4\text{ }\mu\text{m}$ , and moving towards each other in a time of about 1 s.

quantify interaction parameters from individual trajectories, based on the general method of maximum likelihood [21]. Consider a Brownian particle moving in one dimension, with position  $x$ . Its dynamics are given by the Smoluchowski Equation [20]. In general, the diffusion coefficient  $D$ , and applied force  $F$ , may depend on  $x$ . However, over sufficiently short time intervals  $\Delta t$ , the particle samples a region where force and diffusion coefficient are uniform. In this case, the change in the particle position,  $\delta = x(t + \Delta t) - x(t)$ , is given by a Gaussian probability distribution  $p(\delta | \Delta t, F(x), D(x))$ . The mean,  $\mu$ , and standard deviation,  $\sigma$ , of the distribution depend on the force and diffusion coefficient as

$$\mu = \left( \frac{FD}{k_B T} + \frac{dD}{dx} \right) \Delta t, \quad (2)$$

$$\sigma = \sqrt{2D\Delta t}. \quad (3)$$

Smoluchowski's theory is typically used to calculate the motion of particles of known mobility in known potentials. However, it can also be used to infer the force and diffusion coefficient from the statistics of particle trajectories. Consider a discretely sampled one-dimensional trajectory  $\{x_1, \dots, x_N\}$ , where  $x_i$  indicates the coordinate at time  $t_i$ . The force and diffusion profiles are unknown,

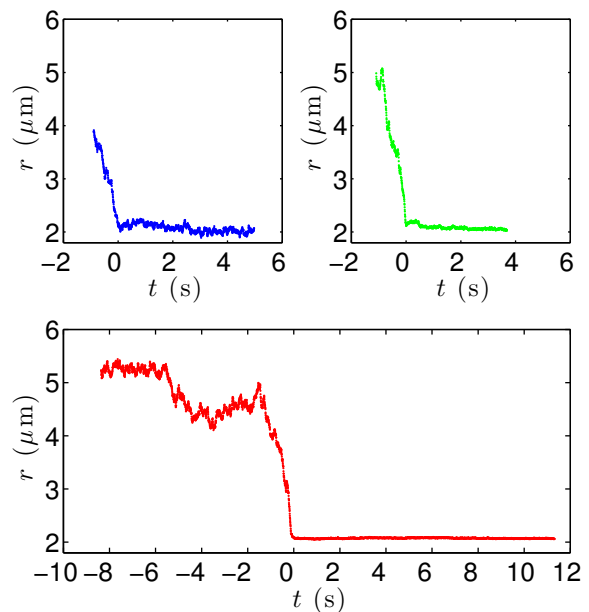


FIG. 2. Representative trajectories of particle pair separations on three different vesicles. All trajectories equilibrate at a distance around  $2\text{ }\mu\text{m}$  in the bound state ( $t \geq 0\text{ s}$ ). Though the red trajectory (Bottom) is mostly flat at  $t \geq 0$ , the blue (Top-Left) and green (Top-Right) trajectories exhibit some slow fluctuations, notably some sort of 'bump' within  $\sim 0.5\text{ s}$  after binding, and a slightly decreasing trend over a few seconds.

but we assume that they can be described by a discrete set of parameters  $\alpha^0 = \{\alpha_1^0, \dots, \alpha_q^0\}$ . For example, in the case of homogeneous force and mobility, this is simply  $\{F_0, D_0\}$  where  $F_0$  and  $D_0$  are constants. Given a trial set  $\alpha = \{\alpha_1, \dots, \alpha_q\}$ , the probability density of observing the trajectory  $\{x_1, \dots, x_N\}$  is

$$\mathcal{P}(\alpha) = \prod_{i=1}^{N-1} p(\delta_i | x_i, \Delta t, \alpha), \quad (4)$$

where  $N$  is the number of sampled timepoints, and the discrete displacements are  $\delta_i = x_{i+1} - x_i$ . In the limit of large trajectories ( $N \rightarrow \infty$ ),  $\mathcal{P}(\alpha)$  is maximum when  $\alpha = \alpha^0$ , as shown in the Supporting Information. In practice, the analysis is more stable numerically if one maximizes a log-likelihood function

$$\mathcal{L}(\alpha) = \frac{1}{N-1} \sum_{i=1}^{N-1} \ln [p(\delta_i | x_i, \Delta t, \alpha)] \quad (5)$$

The main benefit of this approach is that it does not require the construction of an empirical probability distribution, and can be implemented with a single trajectory. The key limitation of this approach is that it requires a model for the spatial dependence of the force and diffusion coefficient.

## FAR-FIELD INTERACTION

We apply the maximum likelihood analysis to estimate the interaction parameters for the three trajectories shown in Fig. 2. We start by restricting our attention to the far-field attractive interaction, laying aside the stably bound portion of the trajectory. As an example, the displacements as a function of interparticle separation for the red trajectory are presented in Fig. 3(Top).

It is important to note that, to our knowledge, there is no theoretical form for the attractive force between micron-sized particles on a tense vesicle [13]. For simplicity, we assumed that the attractive force decays monotonically with separation, and implemented a variety of functional forms that satisfy this minimal criterion. All these functional forms result in equivalent force profiles, as discussed in the Supporting Information. For definiteness, we now assume that the force between the particles has the form

$$F(r) = -\phi K_1 \left( \frac{r}{\beta} \right), \quad (6)$$

where  $K_1$  is the modified Bessel function of the second kind and of order one. Therefore, the force  $F$  depends only on two parameters: a magnitude  $\phi$  and a lengthscale  $\beta$ . Note that this is the expected functional form for tension-dominated interactions of surface-bound spheres subject to an external force [22, 23].

Similarly, there is no appropriate theory for the relative diffusion coefficient of two large beads bound to a lipid membrane, where both the liquid and the membrane contribute [24–27]. Therefore, we assume a simple form for the relative diffusion coefficient: it should be zero in contact and plateau to some constant value at large separations. These basic criteria are satisfied by the form for identical spheres in a viscous fluid [28]:

$$D(r) = D_0 \times \frac{12(r/R_0 - 2)^2 + 8(r/R_0 - 2)}{6(r/R_0 - 2)^2 + 13(r/R_0 - 2) + 2}, \quad (7)$$

where  $D_0$  is the one-particle diffusion coefficient at infinite distance, and  $R_0$  is the hydrodynamic radius of the particle. In a viscous fluid,  $D_0$  and  $R_0$  are related through the original Stokes-Einstein relation. Here, we let them vary independently to accommodate contributions from both the membrane and bulk. Putting together these forms for the force and hydrodynamic drag, the far-field trajectories are characterized by a set of four parameters:  $\{\phi, \beta, D_0, R_0\}$ .

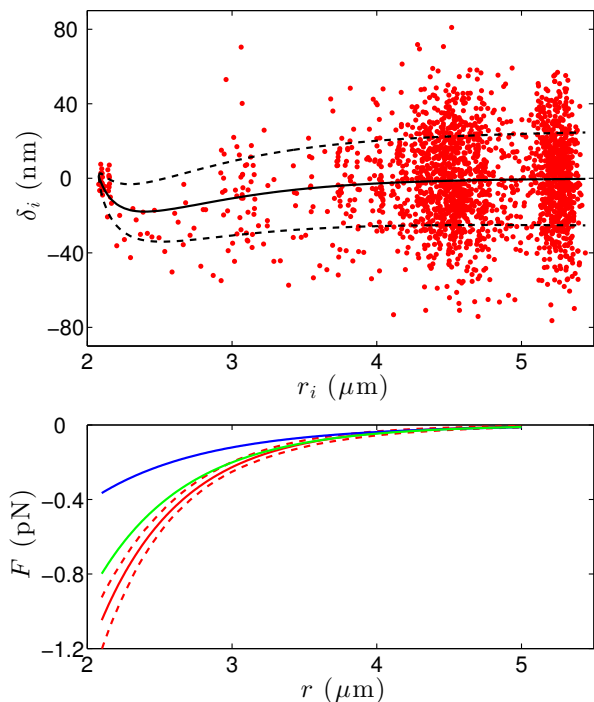


FIG. 3. Displacement and force fits. (Top) Frame-to-frame ( $\Delta t = 4$  ms) displacements  $\delta_i$  as a function of pair separation  $r_i$  for the far-field part of the red trajectory. The red dots represent the experimental data. The solid black line is the maximum likelihood fit for the mean displacement. The dashed lines represent the standard deviation due to Brownian motion ( $\sqrt{2D(r)\Delta t}$ ). (Bottom) Force profiles obtained from the maximum likelihood analysis of the blue, green, and red far-field trajectories. The dashed red lines represent the 25th and 75th percentile of fitted force values (see Supporting Information Text and Fig. S7).

We report the parameter values that maximize the likelihoods for the trajectories in Fig. 2 in Table I. The inferred mean and standard deviation of the frame-to-frame displacement distribution for the red trajectory are plotted on top of the datapoints in Fig. 3(Top). The inferred force profiles for all three trajectories are shown in Fig. 3(Bottom). The forces have maximum values of about 1 pN, and decay over lengthscales of a few microns.

The force profiles for the three pairs of particles appear quite different. To determine if these differences are significant, we estimated the uncertainty in the force profile. We simulated 1000 trajectories with the same number of data points and time intervals as our experiments (see details in the Supporting Information). Even though the interaction parameters are the same in each simulation, each trajectory is different due to the stochastic nature of Brownian motion. For each of these trajectories, we determined the most likely value of the interaction parameters using the same methods as employed with our data. At each separation, we calculated the 25th and 75th percentile values of the force (Fig. S7), plotted as dashed lines about the solid red curve in Fig. 3(Bottom). The uncertainty in the force at each separation is roughly  $\pm 15\%$ . Therefore, the differences in the force profiles across the three trajectories are significant, and presumably due to differences in the membrane tension and the wrapping of the bead by the membrane.

The spatial dependence of the diffusion coefficient is surprisingly well-captured by Eq. 7, with a hydrodynamic radius,  $R_0$ , that is not significantly different from the particle radius,  $R$ , in any of the three trajectories (Table I). However, the limiting value of the diffusion coefficient varies more significantly from particle to particle, perhaps reflecting differences in the extent of wrapping by the membrane.

## NEAR-FIELD INTERACTION

Having analyzed the far-field attraction, we now focus on the pair interaction in the bound state. Significant fluctuations of the interparticle separation are observed, with essentially two characteristic timescales. Notably in

TABLE I. Most likely parameters in the far-field (F.F.), and comparison with results in the near-field (N.F.). The number of significant digits comes from numerical uncertainty in maximization of the likelihood. (\*) See Table II.

	Blue		Red		Green	
	F.F.	N.F.	F.F.	N.F.	F.F.	N.F.
$\phi$ ( $\times 10^{-11}$ N)	0.29	-	2.88	-	1.43	-
$\beta$ ( $\times 10^{-7}$ m)	10.1	-	6.85	-	7.70	-
$D_0$ ( $\times 10^{-14}$ m <sup>2</sup> /s)	8.41	0.26	5.48	0.89	9.85	1.9
$R_0$ ( $\mu$ m)	1.037	(*)	1.038	0.99	1.044	0.89

the first 0.5 s of the bound state, we notice some slow features (see Fig. 2, blue and green), which we attribute to evolving wrapping of the membrane around the particles. After this transition period, the particle separation fluctuates about an apparent equilibrium separation, with a characteristic time corresponding to the bond's time constant of about 5 ms (see Supporting Information). At this point, the particle interaction should be given simply by Hooke's law,  $F(r) = -k(r - r_{eq})$ , with  $k$  the spring constant and  $r_{eq}$  the equilibrium distance.

Assuming these fast fluctuations are thermal in origin, we can reliably extract the spring constant and equilibrium separation using Boltzman statistics:  $k = k_B T / (\langle r_i^2 \rangle - \langle r_i \rangle^2)$ , and  $r_{eq} = \langle r_i \rangle$ , respectively. The results for this method are presented in Table II. As expected, the equilibrium separation of the particle are consistently found to be close to the nominal particle diameter. Interestingly, the measured spring constants span two orders of magnitude. Note that the trajectories with the strongest/weakest forces in the far field have the stiffest/softest interaction in the near field. We suspect that these widely varying stiffnesses depend strongly on the tension and state of wrapping of the particles by the membrane.

Alternatively, the interactions in the bound state can also be extracted from the particle displacements using the maximum likelihood analysis. Using Hooke's Law for the spatial dependence of the force and Eq. 7 for the diffusion coefficient, the interaction parameters are  $\{k, r_{eq}, D_0, R_0\}$ . The most likely values of these parameters are reported in Table II, which allows for a comparison of the results from the two methods.

The values of  $k$  and  $r_{eq}$  from the maximum likelihood analysis agree very well with the values obtained from the Boltzmann statistics analysis. However, the maximum likelihood analysis also yields estimates for the diffusivity and hydrodynamic radius of the particles. The diffusivities are systematically lower than those inferred from the far-field trajectories. This is not surprising, since Eq. 7 does not account for the membrane and should not

TABLE II. Results from the maximum likelihood (M.L.) analysis, and comparison with the Boltzmann statistics analysis (B.S.). The number of significant digits comes from numerical uncertainty in maximization for M.L., and standard statistical uncertainty for mean and variance for B.S. (\*) The analysis returned unreliable values for  $R_0$  for the blue trajectory.

	Blue		Red		Green	
	B.S.	M.L.	B.S.	M.L.	B.S.	M.L.
$k$ (nN/ $\mu$ m)	0.76	0.79	72.3	79.5	8.99	9.4
$r_{eq}$ ( $\mu$ m)	2.06	2.06	2.073	2.0735	2.07	2.0709
$D_0$ ( $10^{-14}$ m <sup>2</sup> /s)	-	0.26	-	0.89	-	1.9
$R_0$ ( $\mu$ m)	-	(*)	-	0.99	-	0.89

capture the full separation dependence of the diffusion coefficient. Further inaccuracies in the diffusion coefficient values may be due to the finite exposure time of the camera, as discussed in the Supporting Information. Note, finally, that the maximum likelihood analysis returned unreliable values for  $R_0$  for the blue trajectory. We expect that this is because beads have not reached a robust equilibrium in the bound state – see the slow continuous downward trend in the separation in Fig. 2.

By integration of the measured force profile, we construct the two-particle membrane-mediated energy landscape for the red trajectory in Fig. 4. The potential depth exceeds  $150 k_B T$ .

## CONCLUSION

We observed long-range attractions between micron-sized functionalized polystyrene spheres strongly adhered to a tense lipid bilayer. Established methods for quantifying interparticle forces proved unapplicable due to the strength of the interaction, and the coupling of the vesicles to optical tweezers. Consequently, we introduced an alternate approach to estimate pair interactions based on a maximum likelihood analysis. Instead of measuring the force at each separation, it estimates the most likely values of a few unknown parameters of a presumed separation dependence of the interaction. Consequently, this approach estimates the force profile with many fewer observations than spatially resolved measurements of the drift velocity and diffusion coefficient [20], and therefore is well-suited to single-trajectory analysis.

While assuming a functional form for the particle interaction reduces the quantity of required data, it introduces systematic errors when the assumed form of the interaction is different from the actual form. In practice,

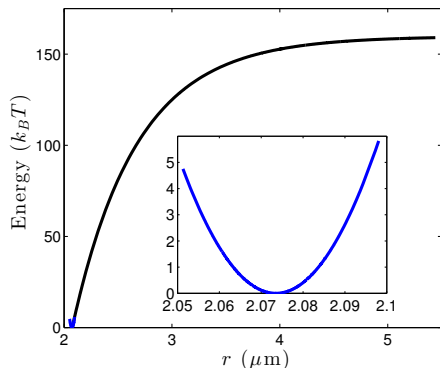


FIG. 4. Plot of the estimated energy landscape as a function of the pair separation. Inset: zoom-in of the near-field part. The binding energy is greater than  $150 k_B T$ , and the strong curvature near equilibrium explains the stiffness of the bound state.

however, we have found that a diverse class of presumed functional forms for the interaction leads to similar values for the magnitude and range of the observed attraction (Fig. S6).

At this point, the origin of such long-range and strong attractions remains unclear. Thermal fluctuations of the membrane can drive attractive Casimir forces between bound particles [13], but on tensionless membranes they are too weak ( $\sim 1$  fN), and should be even weaker on tense vesicles. The membrane's bending energy has been found to induce attractions in a certain regime of high wrapping, with magnitude up to  $\kappa/a \sim 100$  fN on tensionless membranes, but the range of attraction is much smaller than that observed here [14].

In the far-field, we expect interactions to be dominated by membrane tension. In that case, an attractive interaction is expected when a net external force is applied to the particles [23]. Attractive interactions have also been observed in simulations based on the combination of adhesion energy and membrane tension [15].

Given the importance of understanding membrane-mediated interactions for biology, and potential perspectives in colloid engineering, we hope that the results presented here will stimulate the development of new theoretical models.

Further improvements to the experimental approach are also needed. A systematic measurement of particle interactions as a function of membrane tension is essential to a complete understanding of this problem. Interpretation of our results are further complicated by the idiosyncracies of the electroformation process, which produces vesicles with widely varying tensions. Currently, we do not have a convenient way of controlling the membrane tension that is consistent with other elements of the measurement.

The authors thank Jason Merrill, Jin Nam, Frederic Pincet, and Rob Style for helpful discussions. This work was supported by the National Science foundation (CBET 12-36086).

- 
- [1] Alberts B, et al. (2007) *Molecular Biology of the Cell* (Garland Science), 5th Ed.
  - [2] Ishikawa H (1968) Formation of elaborate networks of t-system tubules in cultured skeletal muscle with special reference to t-system formation. *J Cell Biol* 38(1):51-66
  - [3] Saranathan V, et al. (2010) Structure, function, and self-assembly of single network gyroid  $I_{4132}$  photonic crystals in butterfly wing scales. *Proc Natl Acad Sci USA* 107(26):11676-11681.
  - [4] Frost A, et al. (2008) Structural basis of membrane invagination by F-bar domains. *Cell* 132:807-817.
  - [5] Zhu C, Das SL, Baumgart T (2012) Nonlinear sorting, curvature generation, and crowding of endophilin N-bar on tubular membranes. *Biophysical Journal* 102(8):1837-1845.

- [6] Reynwar BJ, et al. (2007) Aggregation and vesiculation of membrane proteins by curvature-mediated interactions. *Nature* 447:461-464.
- [7] Akabori K, Santangelo CD (2011) Membrane morphology induced by anisotropic proteins. *Phys Rev E* 84:061909.
- [8] Canham PB (1970) The minimum energy of bending as a possible explanation of the biconcave shape of the human red blood cell. *Journal of Theoretical Biology* 26(1):61-76.
- [9] Helfrich W (1973) Elastic properties of lipid bilayers: Theory and possible experiments. *Z. Naturforsch.* 28(11):693-703.
- [10] Baumgart T, Hess ST, Webb WW (2003) Imaging co-existing fluid domains in biomembrane models coupling curvature and line tension *Nature* 425:821-824.
- [11] Pouligny B, Martinot-Lagarde G, Grehan G, Gouesbet G, Angelova MI (1994) Stressing phospholipid membranes using mechanical effects of light. *Progr Colloid Polym Sci*, 97:293-297.
- [12] Koltover I, Rädler JO, Safinya CR (1999) Membrane mediated attraction and ordered aggregation of colloidal particles bound to giant phospholipid vesicles. *Phys Rev Lett* 82(9):1991
- [13] Deserno M, Kremer K, Paulsen H, Peter C, Schmid F (2013) Computational studies of biomembrane systems: Theoretical considerations, simulation models, and applications. *Adv Polym Sci* 260:237-284.
- [14] Reynwar BJ, Deserno M (2011) Membrane-mediated interactions between circular particles in the strongly curved regime. *Soft Matter* 7:8567-8575.
- [15] Šarić A, Cacciuto A (2012) Fluid membranes can drive linear aggregation of adsorbed spherical nanoparticles. *Phys Rev Lett* 108(11):118101.
- [16] Angelova MI, Dimitrov DS (1986) Liposome electroformation. *Faraday Discuss Chem Soc* 81:303-311
- [17] Crocker JC, Grier DG (1996) Methods of digital video microscopy for colloidal studies. *J Colloid Interface Sci* 179(1):298-310.
- [18] Prieve DC, Frej NA (1990) Total internal reflection microscopy: a quantitative tool for the measurement of colloidal forces. *Langmuir* 6(2):396-403.
- [19] Neuman KC, Block SM (2004) Optical trapping. *Rev Sci Instrum* 75(9):27872809.
- [20] Sainis SK, Germain V, Dufresne ER (2007) Statistics of particle trajectories at short time intervals reveal fN-scale colloidal forces. *Phys Rev Lett* 99:018303.
- [21] Sijbers J, den Dekke AJR (2004) Maximum likelihood estimation of signal amplitude and noise variance from MR data. *Magnetic Resonance in Medicine* 51(3):586-594.
- [22] Nicolson MM (1949) The interaction between floating particles. *Proc Camb Philos Soc* 45(2):288-295.
- [23] Kralchevsky PA, Nagayama K (2000) Capillary interactions between particles bound to interfaces, liquid films and biomembranes. *Adv Colloid Interface Sci* 85:145-192.
- [24] Di Leonardo R, et al. (2008) Hydrodynamic interactions in two dimensions. *Phys Rev E* 78:31406.
- [25] Petrov EP, Schwille P (2008) Translational diffusion in lipid membranes beyond the Saffman-Delbrück approximation. *Biophys J* 94(5):L41-L43.
- [26] Naji A, Levine AJ, Pincus PA (2007) Corrections to the Saffman-Delbrück mobility for membrane bound proteins. *Biophys J* 93(11):L49L51
- [27] Hormel TT, Kurihara SQ, Brennan MK, Wozniak MC, Parthasarathy R (2014) Measuring lipid membrane viscosity using rotational and translational probe diffusion. *Phys Rev Lett* 112:188101.
- [28] Biancaniello PL and Crocker JC (2006) Line optical tweezers instrument for measuring nanoscale interactions and kinetics. *Rev Sci Instr* 77(11):113702